Properties of the solar granulation obtained from the inversion of low spatial resolution spectra

C. Frutiger[1]**, S.K. Solanki**[1,2]**, M. Fligge**[1]**, and J.H.M.J. Bruls**[3]

[1] Institute of Astronomy, ETH-Zentrum, 8092 Zürich, Switzerland
[2] Max-Planck-Institut für Aeronomie, 37191 Katlenburg-Lindau, Germany
[3] Kiepenheuer-Institut für Sonnenphysik, 79104 Freiburg, Germany

Abstract. The spectra of cool stars are rich in information on elemental abundances, convection and non-thermal heating. Extracting this information is by no means straightforward, however. Here we demonstrate that an inversion technique may not only provide the stratification of the classical parameters describing a model atmosphere, but can also determine the properties of convection at the stellar surface. The inversion technique is applied to spectra of photospheric lines, one recorded at the quiet solar disk center, the other integrated over the whole disk. We find that a model based on a single plane-parallel atmosphere gives unsatisfactory fits to the spectral lines and suffers from considerable uncertainties in the derived temperature stratification. Also, the elemental abundances returned by the inversion are not particularly reliable. These problems are greatly reduced if two atmospheric components, corresponding to granular up- and downflows are allowed for. The best results are obtained if the line profiles and bisectors of a neutral and ionized species are fit and the results are constrained using a simple mass conservation scheme. We find that inversions based on two- and three-component models of disk-integrated spectra give similar results to inversions of disk-center observations, although with somewhat lower accuracy. This similarity is promising for future applications of line profile inversions to the study of late-type stars and in particular their convection.

Key words: line: profiles – radiative transfer – Sun: granulation – Sun: photosphere

1. Introduction

An accurate determination of atmospheric quantities from the analysis of spectral line profiles is one of the main goals of solar and stellar spectroscopy. This aim is rendered difficult by the fact that many physical parameters contribute to the formation of the emergent line profiles. Inversion methods address this problem by simultaneously varying all (or at least many) relevant quantities in a parameterized model of the atmosphere in order to iteratively obtain the best fit to the observed profiles.

Send offprint requests to: C. Frutiger (frutiger@astro.phys.ethz.ch)

Different iteration schemes have been proposed. They differ by the number of free parameters, the amount of physics entering the analysis and various simplifying assumptions needed to reduce the computational effort. Note, however, that all schemes are finally based on a least square fitting procedure.

In the photosphere of the sun and other cool stars overshooting convection plays an important role. In particular, these photospheres are strongly structured by granulation. Convection at the solar surface has been studied in great detail during the past decades (see Spruit et al. 1990 for a review). Numerical simulations provide considerable insight at the expense of a large computational effort (e.g., Nordlund & Stein 1996; Ploner et al. 2000). State of the art models match the best solar observations with great accuracy if the limited spatial resolution of the observations is taken into account (e.g., Nordlund 1984; Lites et al. 1989; Gadun et al. 1999).

Line-profile inversions have the advantage of complementarity to numerical simulations (they do not rely on the same assumption as the simulations), speed (inversions are far less computationally intensive than simulations) and the fact that to a certain extent they allow us to judge the information content of the observations better than the simulations. For example, if a certain simulation reproduces a given set of observations this could either have to do with the fact that the simulation incorporates the relevant physics, or that the observations are not sufficiently sensitive to decide this. The relative speed of inversions makes them of particular interest to stellar applications, e.g., for the analysis of spectra of large samples of stars (from which abundances, turbulence velocity, gravity, temperature stratifications and possibly the granular structure is derived).

A detailed study of stellar granulation based on a comparison of observed and synthetic line profiles was carried out for example by Dravins (1990). This work adopts four-component description of the stellar photosphere to examine the effects of stellar granulation on photospheric line asymmetries and wavelength shifts.

In the present paper we concentrate on the photospheric layers of the quiet sun, in particular on the determination of the temperature stratification and line-of-sight velocity structure imposed by the solar granulation. We address the question of how well our inversion code can unscramble the various in-

fluences of the dynamics on the shapes of the spatially unre-
solved intensity profiles obtained at disk center, and to what
extent an inversion can return the properties of the granulation
from stellar type spectra (observations of the sun as a star). We
present inversions in which the solar atmosphere is divided into
one or more idealized, plane-parallel atmospheres, in the fol-
lowing called components. The single-component models rep-
resent the average quiet sun in the sense of the earlier empirical
models of Gingerich et al. (1971), Holweger & Müller (1974),
Vernazza et al. (1981) and Grevesse & Sauval (1999). The
multi-component models are constructed to describe the gra-
nules and inter-granular lanes, similar to Dravins (1990). In the
first part of the paper we invert spectra obtained at solar disk
center, while in the second part we apply the same inversions
and modeling techniques to spectra integrated over the whole
disk. This allows us to verify the feasibility of applying our
inversion approach to stellar spectra.

2. Observational and atomic data

For our analysis we used the quiet-sun spectral atlases of
Neckel (1994; 1999) for disk center intensities and disk-
integrated normalized fluxes. They were recorded by J. Brault
and his co-workers with the Fourier-transform spectrometer
(FTS) at the McMath-Pierce facility on Kitt Peak. The disk aver-
aged spectra were earlier published by Kurucz et al. (1984), but
have been calibrated using observations of the center-to-limb
variation made by Neckel & Labs (1984).

The spectral lines employed for the inversions are listed
in Table 1, along with the adopted values of the atomic pa-
rameters of importance for our study. We employ both Fe I
and Fe II lines due to their different temperature sensitivities
and formation heights. Column (2) gives the laboratory wave-
lengths. For Fe I lines they are taken from Nave et al. (1994).
Laboratory wavelengths of Fe II lines are generally less ac-
curate, so that the wavelengths of these lines are treated as
free parameters following Bellot Rubio et al. (1999). Column
(3) lists the energy of the lower level of the transition taken
from Sugar & Corliss (1985). Column (4) shows the enhance-
ment factors E (at $T = 5000$ K) over the values of the damping
constant calculated using the simple Unsöld formula for Van
der Waals broadening (Unsöld 1955). For Fe I the collisional
damping parameters are derived from the cross-sections pub-
lished by Anstee & O'Mara (1995), Barklem & O'Mara (1997)
and Barklem et al. (1998). The values for Fe II lines are esti-
mates. Column (5) lists the oscillator strengths, $\log gf$, taken
from the literature without modification[1]. The sources of the
$\log gf$ values are also given.

---

[1] An alternative would have been to use oscillator strengths derived
from additional inversions. Our calculations showed that these modi-
fied strengths may result in better fits, but depend rather sensitively on
the model atmosphere used to derive their values. It is not clear whether
such empirical oscillator strength represent better values than those ob-
tained from furnace measurements or just cover up the inadequacies
of the model atmosphere or spectral data used for the inversions.

Table 1. Atomic data of the inverted spectral lines.

(1)	(2)	(3)	(4)	(5)
Ion	λ^1_{lab} [Å]	χ_e [eV]	E^2	$\log gf$
Fe I	5217.3893	3.2114	2.230	-1.070^4
Fe I	5247.0504	0.0873	3.354	-4.946^3
Fe I	5250.2098	0.1213	3.256	-4.938^3
Fe I	5250.6460	2.1979	1.829	-2.050^3
Fe I	5253.4617	3.2830	2.277	-1.670^3
Fe I	5506.7791	0.9902	2.332	-2.797^3
Fe I	6151.6181	2.1761	2.057	-3.299^3
Fe I	6301.5012	3.6537	2.298	-0.718^4
Fe I	6481.8703	2.2788	2.126	-2.984^3
Fe II	4576.340	2.8443	2.0	-2.90^5
Fe II	4620.521	2.8283	2.0	-3.19^5
Fe II	5234.625	3.2215	2.0	-2.22^5
Fe II	5264.812	3.2307	2.0	-3.23^5
Fe II	6516.080	2.8912	2.0	-3.38^3

[1] Nave et al. (1994), Kurucz & Bell (1995)
[2] Anstee & O'Mara (1995), Barklem & O'Mara (1997)
[3] Fuhr et al. (1988), (Kurucz & Bell 1995)
[4] Bard et al. (1991)
[5] Schnabel et al. (1999)

3. Inversion code

The inversion code used here employs response functions to fa-
cilitate the least-squares fitting of the data. Response functions
were introduced for intensity by Beckers & Milkey (1975) and
used in earlier inversions for example in Mein et al. (1987).
They gained new attraction for the inversion of Stokes pro-
files as proposed by Ruiz Cobo & Del Toro Iniesta (1992),
cf.   Landi Deglinnocenti & Landi Deglinnocenti (1977),
due to the increased speed with which the full stratifi-
cation of various quantities through the solar or stellar
photosphere can be determined, thus making such in-
vestigations more practical. This approach has been
applied to determining the atmospheric structure of
sunspots (Collados et al. 1994; Del Toro Iniesta et al. 1994;
Westendorp Plaza et al. 1997; 1998), solar oscilla-
tions (Ruiz Cobo et al. 1997), the solar chromosphere
(Socas-Navarro et al. 1998), solar magnetic elements
(Bellot Rubio et al. 1997; 1999; Frutiger & Solanki 1998;
Frutiger et al. 1999) and the stellar atmosphere problem
(Allende Prieto et al. 1998).

Our inversions are based on a single- or multi-component
model of the solar atmosphere. For each component the temper-
ature and line-of-sight velocity is modeled as a function of the
logarithmic optical depth $\log \tau$ by spline approximation (splines
under tension) a set of depth-dependent parameters, from a
coarse grid (here we choose 6 grid points per physical quan-
tity) onto a fine depth grid ($\Delta \log \tau = 0.05$). The height of the
former grid points are fixed parameters of the inversions, while
the radiative transfer equation (RTE) is solved on the fine grid.
From the temperature stratifications the other thermodynamic
quantities such as the gas and electron pressure are derived as-

suming hydrostatic equilibrium and LTE (cf. Gustafsson 1973). The micro- and macro-turbulence are assumed to be depth independent. The RTE is solved using a Hermitian method similar to that presented by Bellot Rubio et al. (1999). The emergent synthetic spectra are constructed from a weighted sum over the contributions from the individual components and iteratively fitted to the observed profiles using response functions following Ruiz Cobo & Del Toro Iniesta (1992) and a Levenberg-Marquardt algorithm (cf. Press et al. 1992) that minimizes the merit function

$$\chi^2 = \chi_0^2 + \chi_{\rm reg}^2 \quad \text{where} \quad \chi_0^2 = \sum_{k=1}^{N} \frac{(I_{\rm k,syn} - I_{\rm k,obs})^2}{\sigma_{\rm k}^2}. \quad (1)$$

Here N is the number of all data points fitted, $I_{\rm k,syn}$ are the synthetic intensities (or bisector values), with the index k representing a given spectral line and wavelength (or relative intensity level, in the case of bisectors), $I_{\rm k,obs}$ the corresponding observed quantities and $\sigma_{\rm k}$ the expected uncertainties in the measured profiles.

Of particular importance is the $\chi_{\rm reg}^2$ term we added to the standard merit function. This regularization or penalty term measures the smoothness of the stratifications of all fitted depth-dependent quantities and turned out to be an effective means of damping oscillations in the derived stratifications[2].

Such oscillations are a fundamental problem since, as we show in Sect. 4, the χ^2 value of these oscillating stratifications may be much smaller than the χ^2 value of smoother (and more plausible) stratifications. This may imply that the structure of the model atmosphere may be inadequate to describe the data.

The Levenberg-Marquardt χ^2 minimization algorithm is also not immune to numerical problems causing instabilities. Two of the (as we believe) most important sources of such problems are treated as follows: (a) The inversion of the curvature matrix, which may severely suffer from singularity effects (likely to occur for a large number of free parameters or partially coupled parameters, as in the case of the depth-dependent temperature parameters), is carried out using a special Singular Value Decomposition (SVD) routine combined with an adaptive reordering and rescaling of intermediate results. We tried to further reduce these problems by fitting several spectral lines with different oscillator strength, excitation potential and ionization degree whose line strengths and shapes react differently to (small) changes in the temperature and velocity stratifications. (b) The negative influence of blends on χ^2 is limited by fitting only the (most) unblended part of each line.

---

[2] For appropriately chosen uncertainties $\sigma_{\rm k}$ a rule of thumb states that for a moderately good fit $\chi^2 \approx \nu$ with standard deviation $\approx \sqrt{2\nu}$ ($\nu = N - M$ is the degree of freedom, see Press et al. 1992, Sect. 15.2). A term added to the standard χ^2 of the order of $\sqrt{2\nu}$, as in our case in the form of a regularization term, should therefore not influence the fit. This behavior also allows us to normalize the χ^2 values by the factor $1/\nu$ which enables a direct comparison of the quality of the fit independent of the number of data points and number of free parameters. Therefore all χ^2 values given in the sequel of this paper are given as normalized values.

3.1. Models for the inversion of disk-center observations

We have carried out inversions of solar disk center data using three types of models described below. The models underlying the inversions of disk integrated data are discussed in Sect. 6.2.

1-component models: The granular upflows and inter-granular downflows cannot be described separately. Instead, only average net velocities giving rise to wavelength shifts can be modeled. An alternative, we use here, is the introduction of free central wavelength shifts to account for the net effects due to net line-of-sight velocities. Small-scale velocities are modeled by a micro-turbulence assumed to be depth independent for reasons described in Sect. 5.3. We also include a free Gaussian depth-independent macro-turbulent velocity in our models to account for the actual spread in the up- and downflow velocities. The iron abundance is another free parameter (of most inversions in this paper).

2-component models: Using two components allows us to assign granular upflows and inter-granular downflows to separate components and individually model their depth-dependent velocities as free parameters. The temperature stratification can also be chosen individually for both components. A different (depth-independent, see Sect. 5.3) micro-turbulence in the up- and downflow region is easily accounted for with two free parameters. The free macro-turbulence is assumed to be the same in both components. Refinements of this model, such as imposing the equality between the upward and downward directed mass flux are also possible (see Sect. 5.1). A final final free parameter is the fractional area covered by the downflow.

3-component models: The basic concept of dividing the atmosphere into components attributed with a particular stratification of velocity and temperature can be extended to any number of components. In some cases we have also introduced a third component to describe a surface fraction containing a horizontal flow (see Sect. 5.2).

4. Single-component models at disk center

In a first step we determine a 1-component model of the solar atmosphere, i.e. we are interested in an "average" stratification of the physical properties and intentionally do not try to resolve the different temperatures and velocities associated with the solar granulation.

Best-fit temperature stratifications obtained from the inversion of Fe I lines only as well as of the full set of Fe I and Fe II lines are given in Fig. 1. For the latter case sample best-fit synthetic line profiles are overplotted on observed profiles in Fig. 2.

The results presented in Fig. 1a indicate the inadequacy of the 1-component models: If regularization is turned off χ^2 is minimized (very successfully) at the cost of a physically or at least intuitively sensible stratification. If the regularization is turned on the oscillations are indeed damped, but the smallest achieved χ^2 is 4 times larger. Also, the inversion cannot successfully reproduce the temperature stratification of previous empirical models from the selected line profiles. The
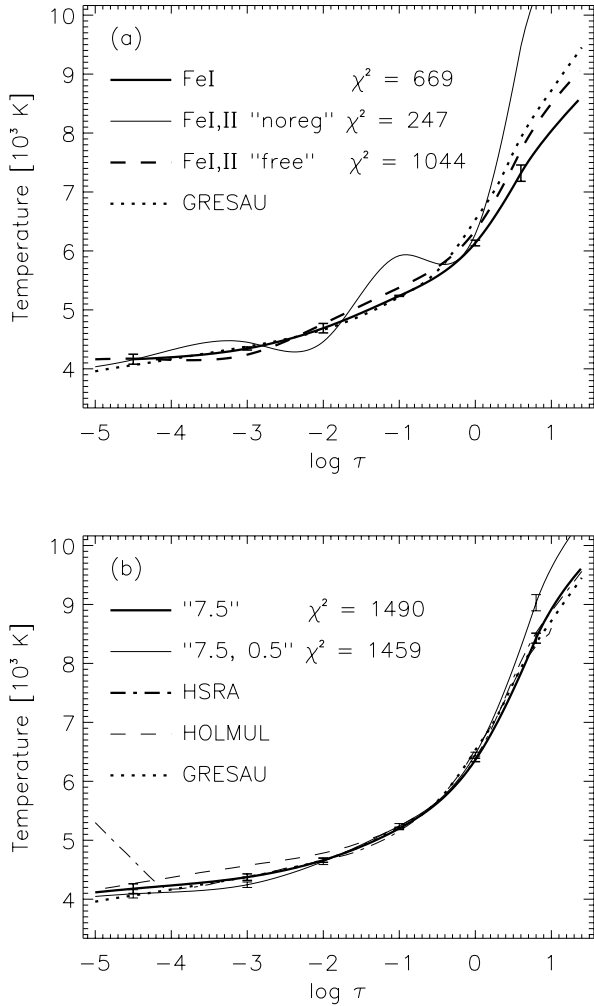
Fig. 1a and b. Best-fit temperature stratifications of 1-component models. **a** shows the results obtained from fits to Fe I lines only (thick solid curve) and fits to Fe I as well as Fe II lines. In the latter case inversions are shown with regularization turned off (solid curve) and turned on (dashed curve). The dotted curve represents the empirical model of Grevesse & Sauval (1999). **b** gives the stratifications for prescribed abundance ($A_{Fe} = 7.50$). Thick curve: free micro-turbulence; thin curve: micro-turbulence fixed at $0.5\,\mathrm{km\,s^{-1}}$. The remaining curves represent stratifications of standard model atmospheres HSRA (Gingerich et al. 1971, dot-dashed), HOLMUL (Holweger & Müller 1974, dashed) and the model of Grevesse & Sauval (1999).

temperature obtained for the deep photospheric layers is too low, while the abundance returned by the code is too high ($A_{Fe} = 7.66 \pm 0.02$ on the usual scale, on which the hydrogen abundance $A_H = 12$). Only if the regularization is switched on (with χ^2_{reg} about $15-25\%$ of χ^2) and the iron abundance is fixed to a standard value are the results in good agreement with common reference atmospheres (e.g., Gingerich et al. 1971, Holweger & Müller 1974). For $A_{Fe} = 7.50$ we obtain the temperature stratifications given in Fig. 1b. For a fixed depth-independent micro-turbulence of $0.5\,\mathrm{km\,s^{-1}}$ the results are similar to those of Allende Prieto et al. (1998) showing cooler up-
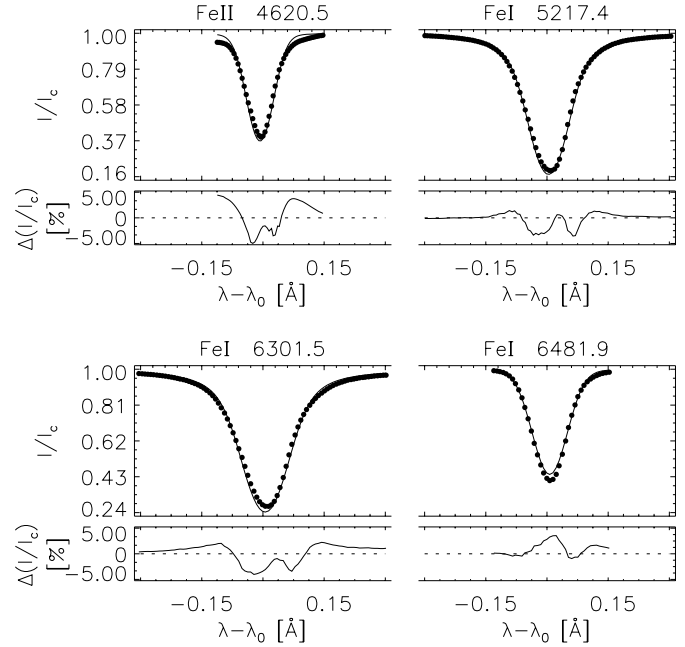
Fig. 2. Best-fit profiles of the 1-component models (with prescribed iron abundance $A_{Fe} = 7.50$ and micro-turbulence $= 0.5\,\mathrm{km\,s^{-1}}$) obtained from fits to Fe I and Fe II lines. In the top and third row of frames thin lines refer to the synthetic spectra, dots to the observed spectra. Row 2 and 4 show the differences between the synthetic and observed profiles on a scale stretched by a factor of 100 for clarity. The fits to the four plotted lines are typical of the whole set of inverted lines.

Table 2. Multi-component models at disk center

Model	Comp	Lines	MC[1]	BIS[2]	N	M
A	2	Fe I	no	no	492	29
B	2	Fe I	yes	yes	614	23
C	2	Fe I, Fe II	no	no	901	35
D	2	Fe I, Fe II	yes	yes	1048	29
E	3	Fe I	yes	yes	614	24
F	3	Fe I, Fe II	yes	yes	1048	30

[1] Mass conservation, [2] fitted bisector

per layers and hotter deeper layers as compared with the reference atmospheres. If we allow the micro-turbulence to vary we obtain $0.77 \pm 0.03\,\mathrm{km\,s^{-1}}$ and the corresponding temperature stratification is in very good agreement with the recent photospheric model of Grevesse & Sauval (1999). Note that the χ^2 values are larger in both cases compared to inversions with free abundances. The fits to the line profiles are correspondingly poor (see Fig. 2).

5. Multi-component models at disk center

5.1. Two-component models

The granular structure of the quiet sun suggests the need for model atmospheres with two or more components that describe the upflowing, downflowing and (possibly) the horizontally

Table 3. Best-fit (depth-independent) parameter values for multi-component models.

Model	α_{hor}	α_{down}	$v_{\mathrm{mic,down}}$ $[km\,s^{-1}]$	$v_{\mathrm{mic,up}}$ $[km\,s^{-1}]$	v_{mac} $[km\,s^{-1}]$	A_{Fe}	χ^2_{reg}	χ^2
A	–	0.23±0.03	0.51±0.32	0.65±0.09	1.12±0.05	7.51±0.04	13	251
B	–	0.28±0.02	1.02±0.10	0.53±0.07	1.15±0.04	7.53±0.03	15	231
C	–	0.23±0.03	0.36±0.21	0.63±0.07	1.30±0.04	7.55±0.02	46	490
D	–	0.29±0.02	0.72±0.02	0.50±0.04	1.40±0.04	7.56±0.02	13	491
E	0.43±0.02	0.34±0.03	1.02±0.07	0.52±0.05	0.80±0.07	7.53±0.03	9	189
F	0.36±0.04	0.35±0.01	0.78±0.10	0.48±0.07	1.24±0.06	7.55±0.02	19	447

flowing plasma, respectively. In the simplest case we consider only two components. The temperatures, the line-of-sight velocities, the free depth-independent micro-turbulence and the fractional contribution to the emergent intensities are derived for both components. As a consequence the total number of free parameters increases to values as high as 35. In view of this large number of free of parameters we carry out some inversions with further constraints:

– We also invert the line bisectors with the goal of improving the determination of the line-of-sight velocities
– We reduce the number of free parameters by adding a physical constraint in the form of a simple mass conservation scheme, where the total upflowing mass is forced to be equal to the downflowing mass. Hence at any given (geometrical) height in the atmosphere the following equation must be satisfied:

$$\alpha_{\mathrm{up}} \cdot \rho_{\mathrm{up}}(z) \cdot v_{\mathrm{los,up}}(z) = \alpha_{\mathrm{down}} \cdot \rho_{\mathrm{down}}(z) \cdot v_{\mathrm{los,down}}(z) \quad (2)$$

with $\alpha_{\mathrm{up}}(\alpha_{\mathrm{down}})$ being the fractional area coverage of upflows (downflows), $\rho_{\mathrm{up}}(\rho_{\mathrm{down}})$ the corresponding density and $v_{\mathrm{los,up}}(v_{\mathrm{los,down}})$ the corresponding line-of-sight velocity. The free velocity $v_{\mathrm{los,down}}$ is given on a logarithmic optical depth grid, but the mass conservation is imposed on a common geometrical depth grid). This description of the line-of-sight velocity as a function of depth is new (The 4-component model by Dravins (1990) has depth independent velocities and a correspondingly simpler mass conservation scheme).

To test the effectiveness of these extensions we carried out a number of inversions of the same data set, but with mass-conservation switched on or off, with or without fitting of line bisectors, fits to Fe I lines alone or fits to Fe I and Fe II.

Table 2 provides an overview of the ingredients of the inversions, together with the final χ^2. In this section we discuss models A-D. The best-fit temperatures and velocities obtained from the 2-component models are shown in Fig. 3. The best-fit values of the remaining free parameters are listed in Table 3.
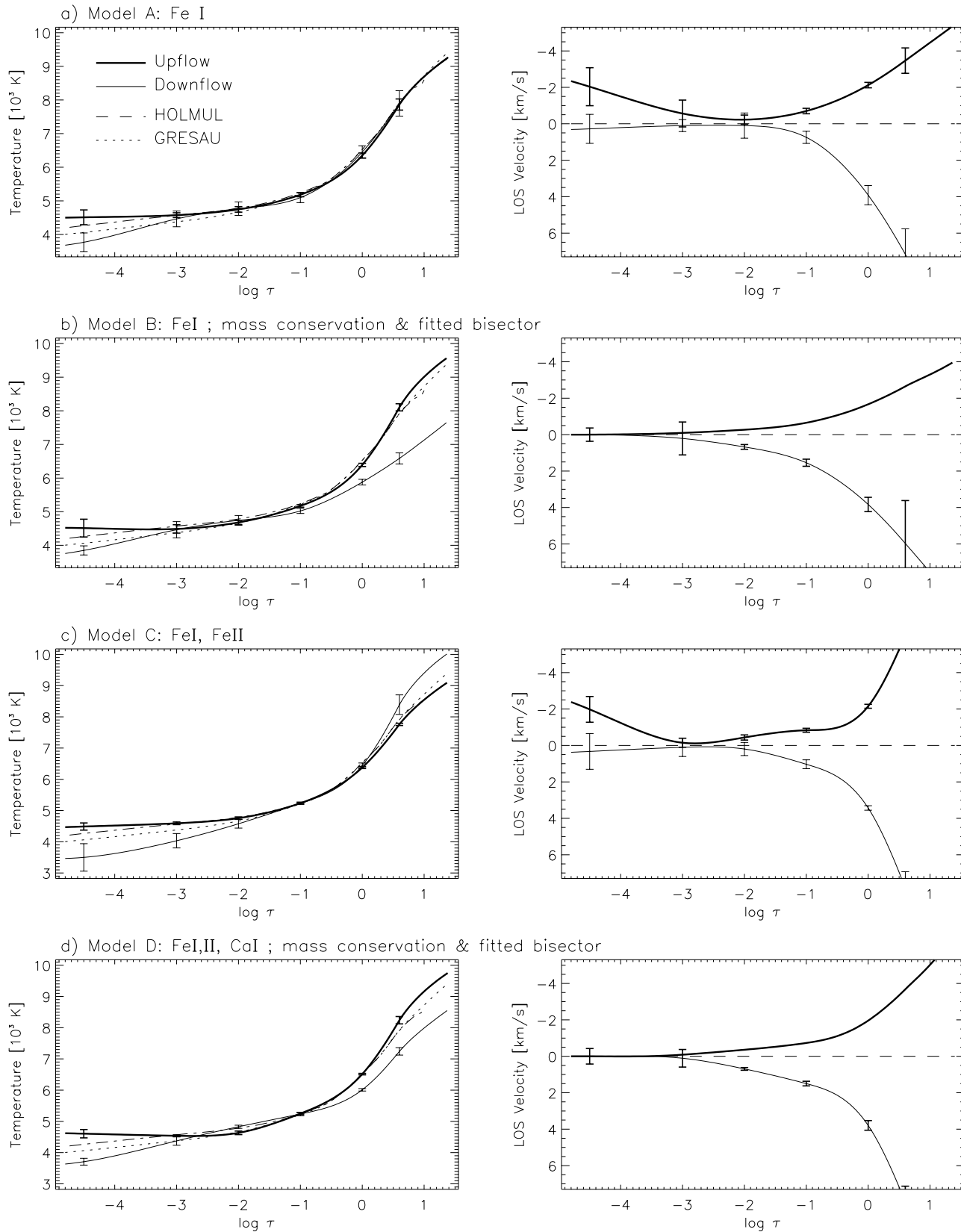
The stratifications of the temperature and velocity in Fig. 3a indicate that the observed Fe I lines profiles do not on their own contain enough information to constrain the up- and downflow component reliably. Note, e.g., that at the continuum-forming level the downflowing component has practically the same temperature as the upflow, contradicting the observational result that

downflow lanes are darker than upflowing granules. In other words minimizing the χ^2 merit function without further constraints fails to return the correct granular structure. The additional fitting of bisectors helps somewhat, but not sufficiently (we deduced this from additional inversions not discussed here further), nor does the inclusion of the Fe II lines in the inversions, as can be seen by considering Fig. 3c. Now the downflow is even hotter and brighter than the upflow.

The additional incorporation of the mass-conservation scheme given by Eq. (2) leads to a great improvement, as can be seen by considering Figs. 3b and 3d. Now the downflow is indeed cooler around $\log \tau = 0$. According to Table 3, the area covered by the downflow is also significantly smaller than the upflow area, with downflow velocities correspondingly larger than the upflowing (negative) velocities (see Fig. 3). This feature is also in agreement with observations. The models with mass-conservation return a larger micro-turbulence in the downflowing region than in the upflowing region, in agreement with the findings of Nesis et al. (1992). Comparing the last columns of Table 2 with the χ^2 values given in Fig. 1 reveals that the 2-component models fit the observed spectra (with or without their bisectors) significantly better than the simple 1-component models. The exception is the 1-component model without regularization, which still has a lower χ^2. This suggests that even the 2-component models, although a great improvement, are not a completely adequate description of the solar photosphere, as mirrored by the selected spectral lines. Note that only a small amount of regularization (χ^2_{reg} typically 5 percent of χ^2) is now needed to get smooth results. The iron abundance returned by the inversions is also close to the standard values, suggesting that in cool stars inversions return more reliable abundances on the basis of 2-component models than for 1-component ones.

5.2. Three components at disk center

The 2-component models are incomplete in the sense that they do not allow for a fraction of the solar surface that is free of vertical flows. It may be associated with horizontal flows. In a next step we therefore introduce an additional component that is at rest when observed at disk center. In order to keep the number of free parameters within bounds we derive the thermodynamical stratifications of the new component from the other two, as described below. Hence, only the fractional area coverage of the third component is a new free parameter. We require

a) Model A: Fe I

b) Model B: FeI ; mass conservation & fitted bisector

c) Model C: FeI, FeII

d) Model D: FeI,II, CaI ; mass conservation & fitted bisector

Fig. 3a–d. Best-fit atmospheres obtained from inversions using different 2-component models. The solid thick curves refer to the upflowing component (negative velocities), while the solid thin curves refer to the downflowing component. Error bars are shown at the optical depths at which free parameters are located. The dotted and dash-dotted curves serve to facilitate the comparison between the models. They represent the temperature stratification according to standard 1-component atmospheres (Grevesse & Sauval 1999 and Holweger & Müller 1974, respectively).
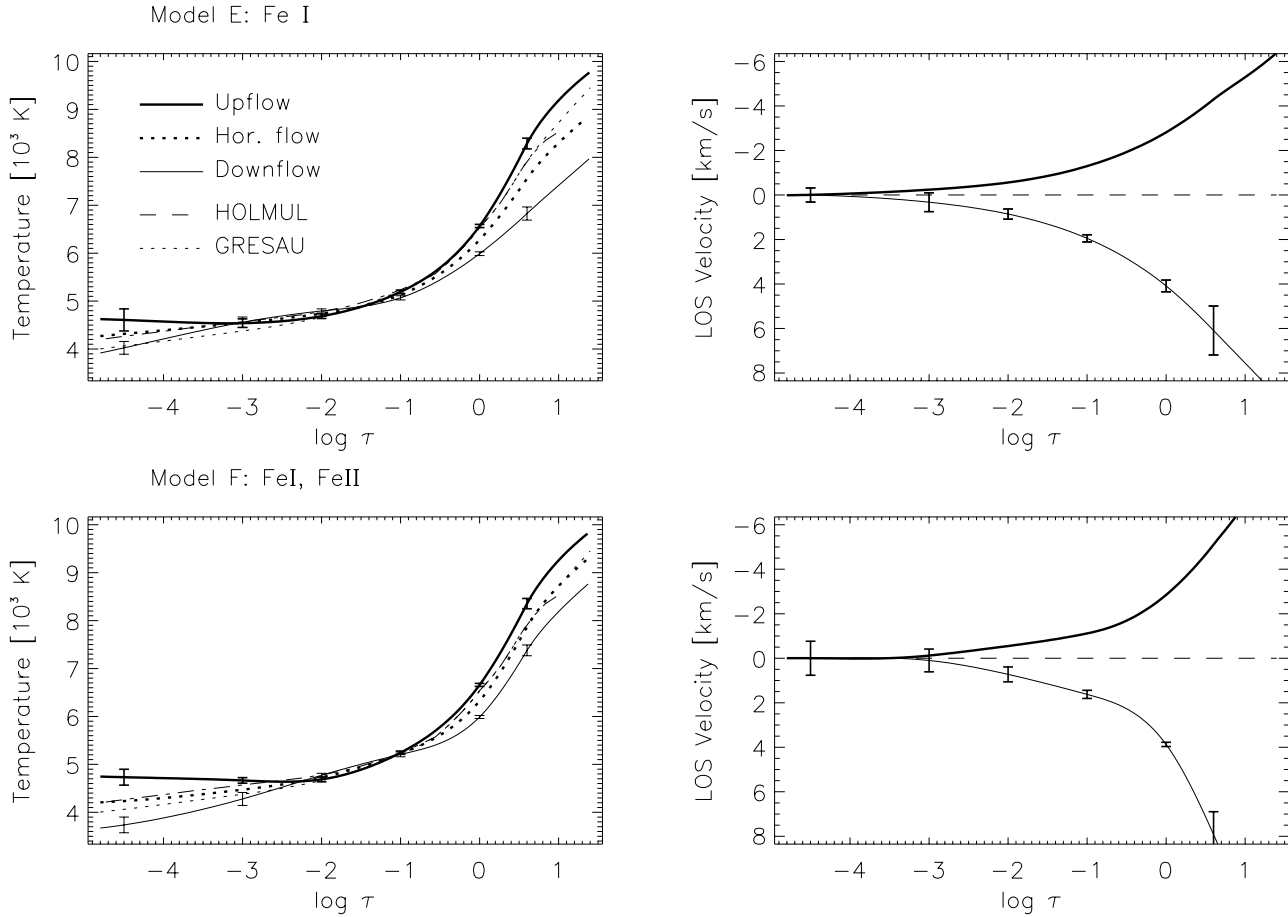
Fig. 4. Best-fit temperatures and line-of-sight velocities obtained from the 3-component models E and F. Thick solid curves refer to the upflow component, thin solid curves to the component harboring a downflow. The thick dotted curves show the average temperature of the two stratifications, corresponding to the third component.

$$T_{\mathrm{hor}}(\tau) = [T_{\mathrm{down}}(\tau) + T_{\mathrm{up}}(\tau)] / 2$$
$$v_{\mathrm{mic,hor}}(\tau) = [v_{\mathrm{mic,down}}(\tau) + v_{\mathrm{mic,up}}(\tau)] / 2$$

so that the emergent intensity is

$$\boldsymbol{I} = (\alpha_{\mathrm{down}}\,\boldsymbol{I}_{\mathrm{down}} + \alpha_{\mathrm{up}}\,\boldsymbol{I}_{\mathrm{up}})(1 - \alpha_{\mathrm{hor}}) + \alpha_{\mathrm{hor}}\,\boldsymbol{I}_{\mathrm{hor}} \qquad (3)$$

where the subscript 'hor' indicates the third component representing the surface area covered by predominantly horizontal flows.

The inversions based on 3 atmospheric components are listed in Table 2 (models E and F), the best-fit atmospheric stratifications and height-independent parameters are presented in Fig. 4 and Table 2, respectively. As expected, these models are able to further reduce the final χ^2 values, although not by a large amount. The results are very similar to the 2-component model with a fast downflow covering about half the surface area[3] In contrast to the 2-component model the results obtained from fits

---

[3] Remember that in the 3-component models the true fraction harboring a downflow is $\alpha_{\mathrm{down,true}} = (1 - \alpha_{\mathrm{hor}})\alpha_{\mathrm{down}}$ (see Eq. 3). As a consequence the downflows cover, as expected, a smaller area than in the corresponding 2-component model ($\alpha_{\mathrm{down,true}} = 0.19$ for model E and $\alpha_{\mathrm{down,true}} = 0.22$ for model F, respectively).

to only Fe I lines are now in good agreement with those from the full list of both Fe I and Fe II lines. Once again the agreement between the derived abundances and standard values is satisfactory. The best-fit line profiles obtained from inversion F are plotted in Fig. 5 along with the observed profiles. The fits to the line bisectors are also plotted. As expected from the lower χ^2 the fits are general better than those obtained with single component models (compare with Fig. 2). The two lines exhibiting the poorest fits, Fe II 4620.5 Å and Fe II 5264.8 Å, may both suffer from inaccurate $\log gf$ values. The former also seems to be more strongly affected by blends than the other lines in our sample.

5.3. Micro-turbulence

Nordlund (1984) showed that synthetic spectra from numerical simulations of solar granulation reproduce the observed Fe I lines poorly if the velocity field is set to zero but nicely fit the observations once the granular velocity field is included, without any additional micro-turbulence broadening. Within the context of the simple model atmospheres used here, however, there is a clear need for micro- and macro-turbulence broadening. The
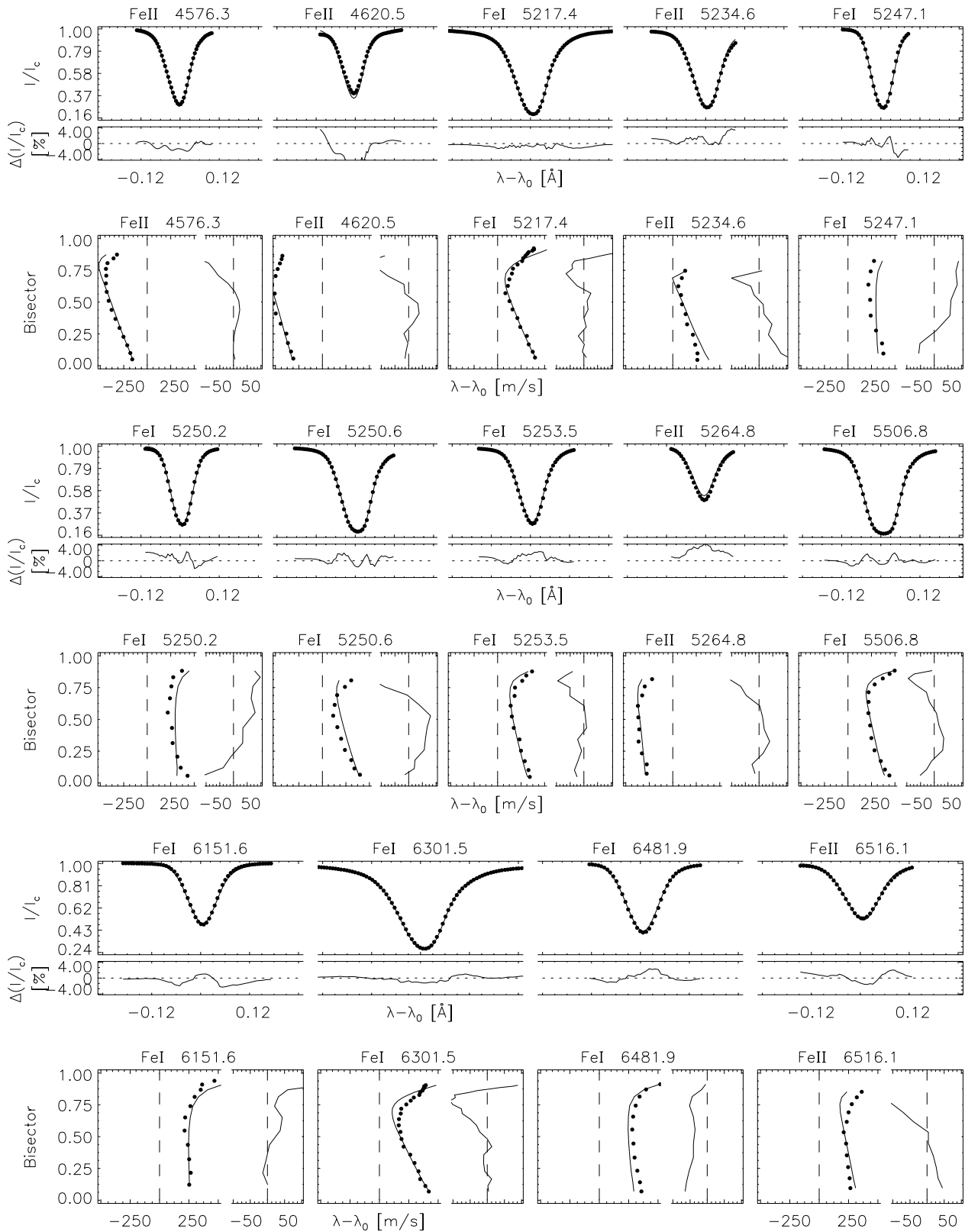
Fig. 5. Observed and best-fit intensity profiles obtained using the 3-component model F. In the I/I_c and bisector panels solid lines refer to the synthetic spectra, dots to the observed data. The $\Delta(I/I_c)$ subpanels just below each intensity profile show the difference between observed and synthetic profiles on an expanded scale. Similarly, to the right of each line-bisector is the difference between the observed and synthetic bisector, this time on an expanded wavelength scale. Bisectors and the corresponding differences are given in velocity units. The vertical dashed lines mark the position of the laboratory wavelength and zero-difference, respectively.
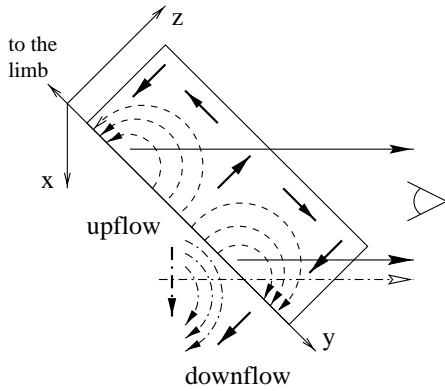
Fig. 6. Cut through a schematic 2(3)-component model of a granular cell observed at $\mu = 0.71$. Thick arrows refer to the components with an upflow (granule), downflow (intergranular lanes) and a horizontal flow. The dash-dotted arrows (not lying in the plane of cut) exhibit the 3-dimensional structure of the flow field which must be taken into account (see Sect. 6.2 for details).

small-scale variations in temperature and line-of-sight velocity present in the real sun obviously cannot be adequately described by a small number of components, even if the LOS velocity is allowed to vary freely with optical depth.

Previous studies revealed a large micro-turbulence in the deep photosphere ($\xi = 2 \text{ km s}^{-1}$ at $z = 0 \text{ km}$) which decreases with height to about $\xi = 0.8 \text{ km s}^{-1}$ at the temperature minimum and increases again in the chromosphere (Canfield 1976; Vernazza et al. 1981). Similar results were obtained by inversions carried out by Ruiz Cobo et al. (1997). Inversions we carried out with a free depth-dependent micro-turbulence basically return the same stratification. The estimated errors returned by the inversion code reach several km s^{-1}, however, and do not inspire much confidence in this result. Our simple 2- and 3-component models may not allow the simultaneous extraction of the temperature-, velocity- and micro-turbulence stratification from the employed spectra. Since the best-fit χ^2 was only marginally improved using a depth-dependent micro-turbulence we decided to use the simpler approximation of a depth-independent micro-turbulence for our calculations.

6. The sun as a star

In this section we investigate the fidelity of the inversion technique when applied to disk integrated spectra. For the sun we are in the favorable position that the results obtained from inversions of disk integrated spectra and disk-center data can be easily compared and the former can be tested prior to an application to other cool stars, which will be the subject of a future paper. A similar investigation was carried out by Allende Prieto et al. (1998) using a single component model and a different set of spectral lines. We thus extend their analysis to encompass multi-component models. Note, that we have also carried out inversions of disk-integrated data using 1-component models. The results are compatible with those obtained from disk-center data. We do not discuss these inversions further in favor of those based on 2-component models.

6.1. Synthesis of disk-integrated fluxes

The main consideration for the calculation of the spectrum of the sun as a star is the appropriate averaging of spectra originating from different parts of the solar disk. With this in mind we compute the intensity profiles for a number (n_μ) of μ values ($\mu = \cos\theta$, with θ being the angle between the line-of-sight and the surface normal). Then, after appropriate weighting, we add these profiles together while taking into account their wavelength shifts due to stellar rotation. To achieve an accurate disk-integration with a relatively small number n_μ we divided the disk into 9 azimuthal sectors of equal projected area to each of which an "average" profile $I(\mu')$ with "optimum" μ' is assigned (see Bruning 1984).

6.2. Two-component, disk-integrated inversions

When a granule is observed at an angle to the vertical its horizontal velocity component also influences the line profiles. Here we discuss, how we treat further complications when calculating profiles at $\mu < 1$. Fig. 6 shows a vertical cut through a schematic granular cell observed at $\mu = 0.71$. The schematic flow field of the granule is represented by the dashed curves (in the plane containing the line-of-sight) and the dot-dashed lines curves in a plane perpendicular to the former. Thick arrows indicate the schematic breakdown of this velocity field into purely vertical and horizontal velocities. Each of the thin long arrows indicate contributions to the emergent intensities from different layers with mainly vertical and mainly horizontal velocities if the horizontal size of the granule is comparable to the vertical extent of the line formation region. Consequently, our multi-component approach also implicitly assumes that granules have a sufficiently large horizontal size. Depth-dependent velocities perpendicular to the surface are modeled with free parameters as at disk-center with the exception that we now have to take into account the correct projection onto the line-of-sight when calculating the intensity profiles $I(\mu)$ for different μ. Velocities parallel to the surface (which do not play a role at disk-center) now become important. However, since their line-of-sight components are equally strong in the directions towards the observer and away from him, the horizontal flows mainly influence the line width and not the line-shifts or asymmetry. Hence they are taken into account by a radial-tangential depth-independent macro-turbulence (see Gray 1975; 1992, Chap. 18). Mind that horizontal velocities perpendicular to the plane show in Fig. 6 do not contribute to the line-broadening (such velocities are indicated by the dot-dashed curves). For simplicity we neglect this surface fraction during the inversion but must bear it in mind when discussing the results.

We have introduced two new parameters: A_T, the fraction of the stellar surface presumed to harbor a tangential motion and ζ_T, the (depth-independent) macro-turbulent velocity describing the horizontal velocities parallel to the surface. (The Gaussian macro-turbulence used in disk-center inversions is replaced by a radial turbulent velocity ζ_R and associated fractional area coverage $A_\text{R} = 1 - A_\text{T}$). We are aware that in this manner
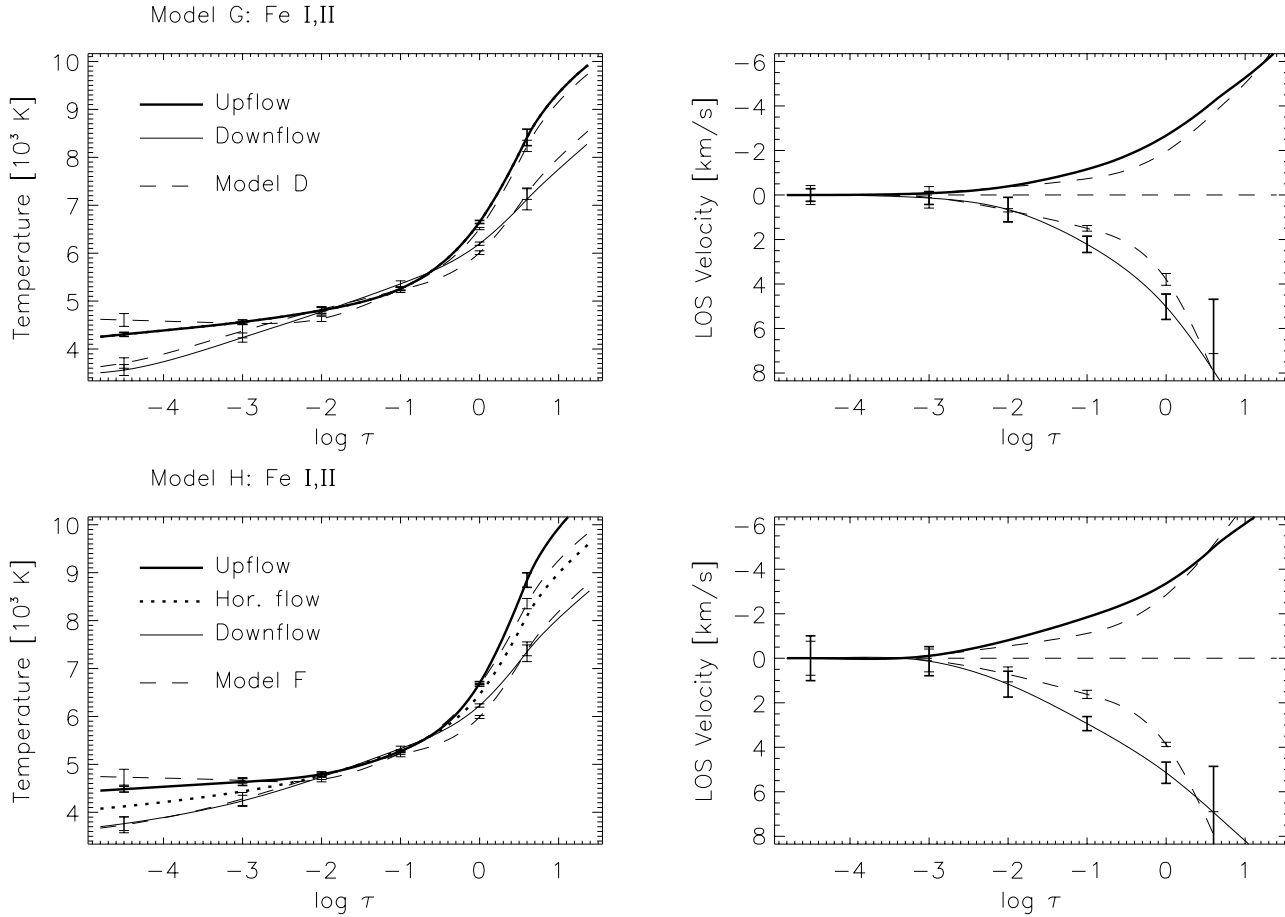
Fig. 7. Best-fit atmospheric stratifications obtained from disk-integrated spectra (solid lines) together with the results obtained from the corresponding models and data at the disk center (dashed lines). See the caption of Fig. 3 for more details.

Table 4. Multi-component models for the inversion of disk-integrated spectra together with best-fit χ^2 values.

Model	Comp.	Lines	MC+BIS	N	M	χ^2
G	2	Fe I, Fe II	yes	1023	30	248
H	3	Fe I, Fe II	yes	1023	31	236

we are neglecting the possible effects due to a depth dependence of the strength of horizontal flows.
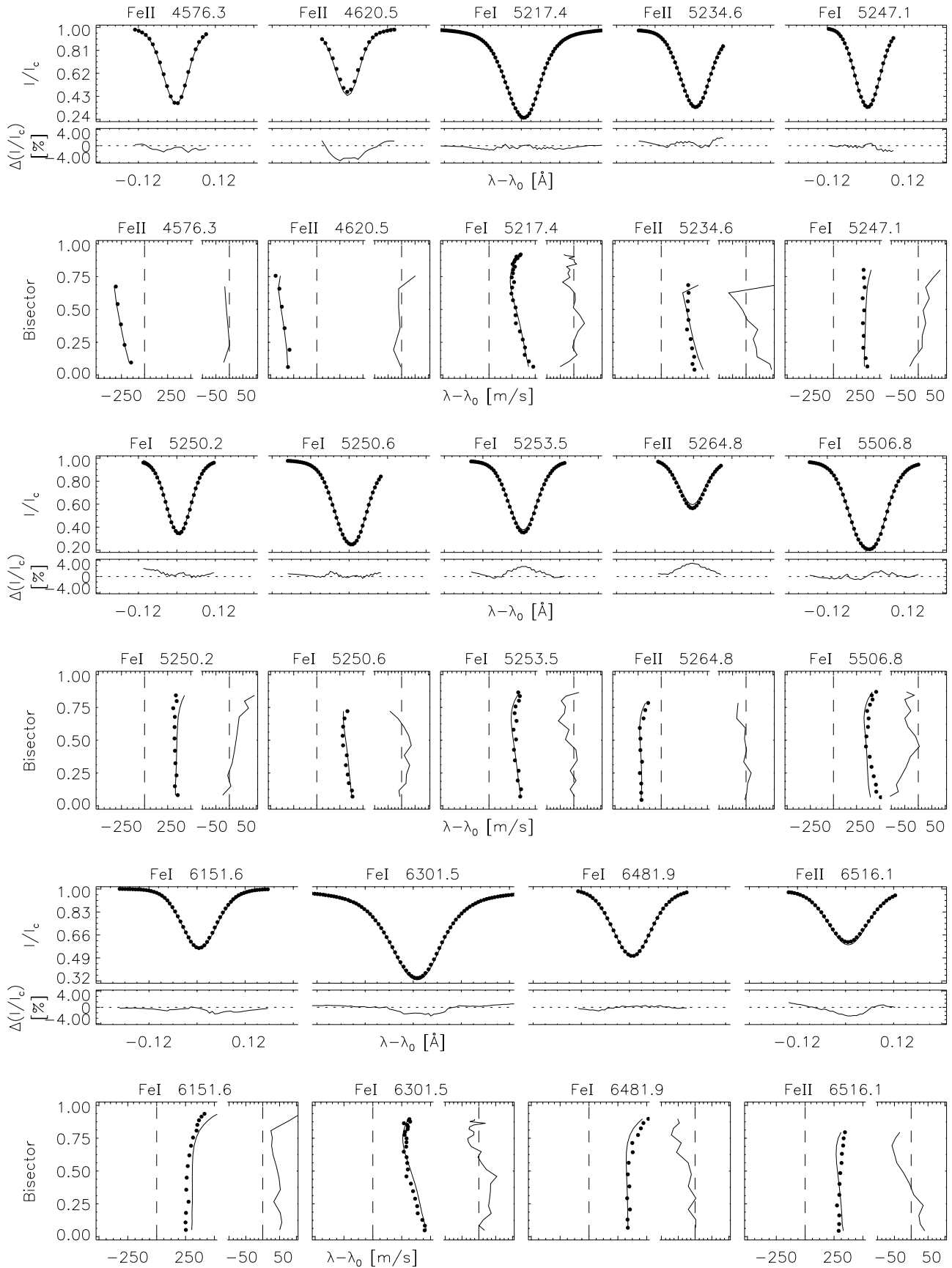
7. Results of inversions of disk-integrated data

We discuss here the results of two inversions whose ingredients are given in Table 4. Except for the macro-turbulent broadening these two models correspond to models D and F used for the inversions of disk-center data.

Best-fit atmospheres obtained from the inversions are displayed in Fig. 7. The remaining best-fit parameters are listed in Table 5, while Fig. 8 exhibits the quality of the fit returned by the 3-component model H. The results of the two models agree well with each other and are also generally in good agreement with those obtained at disk center. The inversions return basically the same temperature structure and a similar velocity

field. The curves do not always agree within the error bars, but it is worth noting that all estimated errors given in this work are 1-dimensional statistical errors which generally underestimate the "true" uncertainties in the obtained results, due to the possible coupling between different free parameters. A comparison with the results obtained from the 4-component model of Dravins (1990) is difficult, since the velocity field is treated rather differently. We will present a detailed comparison of these earlier results with the results of our inversions including those of observed spectra of α-Cen A and α-Cen B, in an upcoming paper.

Columns (4) and (5) of Table 5 list the micro-turbulence in the up- and downflow component and reveal, in agreement with the results at disk center, a higher turbulent velocity in the downflow. Columns (6) and (7) give the macro-turbulent velocities (as obtained from the radial-tangential model). Note that the values of the radial macro-turbulence (ζ_R) and the horizontal turbulence (ζ_T) cannot be directly compared with the Gaussian macro-turbulent velocity at disk center. At first sight the fact that $\zeta_R > \zeta_T$ seems to be in conflict with the results obtained from numerical simulations (e.g. Stein & Nordlund 1998) which show larger horizontal velocities than vertical velocities above the $\log \tau = 0$ surface. The

Fig. 8. Same as Fig. 5, but for synthetic profiles resulting from model H (solid) and disk-integrated data (dots).

Table 5. Best-fit (depth-independent) values from the inversion of disk-integrated spectra.

Model	α_{hor}	α_{dn}	$v_{mic,up}$ [km s^{-1}]	$v_{mic,dnwn}$ [km s^{-1}]	ζ_R [km s^{-1}]	ζ_T [km s^{-1}]	A_{Fe}
G	*0.5*	0.31±0.02	0.66±0.05	0.84±0.08	4.01±0.15	2.80±0.16	7.61±0.02
H	0.30±0.07	0.36±0.02	0.61±0.07	0.94±0.09	3.31±0.16	2.34±0.38	7.59±0.02

Table 6. Corrected laboratory wavelengths of Fe II lines

$\lambda_{lab,kur}$ [Å]	$\lambda_{ref,this\ work}$ [Å]	$d\lambda$ [km s^{-1}]
4576.3400	4576.3330±0.0005	−0.459±0.033
4620.5210	4620.5127±0.0006	−0.536±0.041
5234.6250	5234.6251±0.0006	+0.007±0.036
5264.8120	5264.8060±0.0008	−0.339±0.047
6516.0800	6456.3842±0.0003	+0.109±0.012

obtained value for the tangential turbulence, however, must be interpreted as a spatial average over the line-of-sight component of velocities parallel to the surface but pointing in different directions around the axis of the granular cell (see, e.g., the dot-dashed velocity vector in Fig. 6). As a consequence the horizontal velocities are in reality expected to be about 1.6 times larger than the average value. The reason for the smaller values of both ζ_R and ζ_T obtained from three components as compared to the values obtained from the 2-component model is the different weight entering Gray's radial-tangential formula. In the 2-component model we have set $A_R = A_T = 0.5$ whereas the 3-component model returned $a_{hor} = A_T = 0.3$ ($A_R = 1 - A_T = 0.7$).

The abundances of iron listed in column 8 of Table 5 are slightly larger than those obtained at disk center, and differ by a greater amount from the literature value. Hence the spread of the derived abundances is larger when integrated spectra are inverted.

8. Laboratory wavelengths of Fe II

As mentioned in Sect. 2 the laboratory reference wavelengths of all Fe II lines are free parameters of all inversions using models C and E-H. The best-fit values obtained from the inversions using these models are summarized in Table 6: Column (1) gives the wavelengths from Kurucz & Bell (1995), column (2) the mean wavelengths calculated from the values returned by the inversions and column(3) the corresponding shifts in velocity units. These shifts are in good agreement with the results of Bellot Rubio et al. (1999) and Frutiger et al. (1999).

9. Summary and conclusions

We have presented an analysis based on the inversion of high S/N, high spectral resolution, but low spatial resolution solar spectra to derive the photospheric stratifications in granules and intergranular lanes. The best-fit results are obtained when several Fe I/Fe II line profiles as well as their bisectors are fit us-

ing a small number of plane-parallel atmospheric components and mass conservation between up- and downflows is imposed. Physical constraints of this type were earlier introduced by Frutiger & Solanki (1998) into the inversion of Stokes V spectra (net circular polarization) from active region plage. Interestingly, inversions that take the inhomogeneous structure of the photosphere into account return values of the iron abundance closer to currently accepted values than those that do not.

The present investigation is of interest for inversion-based studies of late-type stars. The inversion approach provides a simple way of deriving the fundamental parameters (T_{eff}, abundances, etc.) of stars, as demonstrated by Allende Prieto et al. (1998), but it may also allow such investigations to be extended in a natural manner to include the effects of granular convection on the atmosphere and thus the line profiles. The demonstration given in this paper that the temperature and velocity stratifications obtained by the inversion of disk-integrated spectra are very close to those obtained from the inversion of data from solar disk center promises that the properties of stellar granulation can be studied by inverting data with sufficiently high S/N ratio and spectral resolution. These inversions are complimentary to numerical simulations such as those of Nordlund & Dravins (1990), Dravins & Nordlund (1990a;b) for the study of stellar convection. Finally, our results also have some bearing on the empirical modeling of unresolved, small-scale solar magnetic elements and their surroundings. The importance of up- and downflows in the non-magnetic vicinity of small magnetic structures is evident, but has not yet been taken into account adequately (since usually only a downflow is considered, but see Briand & Solanki 1998).

References

Allende Prieto C., Ruiz Cobo B., García López R.J., 1998, ApJ 502, 951
Anstee S.D., O'Mara B.J., 1995, MNRAS 276, 859
Bard A., Kock A., Kock M., 1991, A&A 248, 315
Barklem P.S., O'Mara B.J., 1997, MNRAS 290, 102
Barklem P.S., O'Mara B.J., Ross J.E., 1998, MNRAS 296, 1057
Beckers J.M., Milkey R.W., 1975, Sol. Phys. 43, 289
Bellot Rubio L.R., Ruiz Cobo B., Collados M., 1997, ApJ 478, L45
Bellot Rubio L.R., Ruiz Cobo B., Collados M., 1999, A&A 341, L41
Briand C., Solanki S.K., 1998, A&A 330, 1160
Bruning D., 1984, Ph.D. thesis, Univ. New Mexico
Canfield R., 1976, Sol. Phys. 50, 239
Collados M., Pillet V.M., Cobo B.R., et al., 1994, A&A 291, 622
Del Toro Iniesta J.C., Tarbell T.D., Ruiz Cobo B., 1994, ApJ 436, 400

Dravins D., 1990, A&A 228, 218

Dravins D., Nordlund Å., 1990a, A&A 228, 203

Dravins D., Nordlund Å., 1990b, A&A 228, 184

Frutiger C., Solanki S.K., 1998, A&A 336, L65

Frutiger C., Solanki S.K., Fligge M., Bruls J., 1999, in K. Nagendra, J. Stenflo (eds.), Solar polarization, Kluwer, Dordrecht, p. 281

Fuhr J.R., Martin G.A., Wiese W.L., 1988, J. Phys. Chem. Ref. Data 17, Suppl 4

Gadun A.S., Solanki S.K., Johannesson A., 1999, A&A In press

Gingerich O., Noyes R., Kalkofen W., Cuny Y., 1971, Sol. Phys. 18, 347

Gray D.F., 1975, ApJ 202, 148

Gray D.F., 1992, The observation and analysis of stellar photospheres, Cambridge University Press, 2nd ed.

Grevesse N., Sauval A.J., 1999, A&A 347, 348

Gustafsson B., 1973, Uppsala Astron. Obs. Ann. 5, no. 6

Holweger H., Müller E., 1974, Sol. Phys. 39, 19

Kurucz R.L., Bell B., 1995, Harvard-Smithsonian Center for Astrophysics, CD-ROM No. 23

Kurucz R.L., Furenlid I., Brault J., Testermann L., 1984, Solar Flux Atlas from 296 to 1300nm, Harvard University Press

Landi Degl'Innocenti E., Landi Degl'Innocenti M., 1977, A&A 56, 111

Lites B., Nordlund Å., Scharmer G., 1989, in R. Rutten, G. Severino (eds.), Solar and Stellar Granulation, Reidel, Dordrecht, pp. 349–357

Mein P., Mein N., Malherbe J.M., Dame L., 1987, A&A 177, 283

Nave G., Johansson S., Learner R.C.M., et al., 1994, ApJS 94, 221

Neckel H., 1994, in C. Fröhlich, H. Hudson, S. Solanki (eds.), The Sun as a Variable Star: Solar and Stellar Irradiance Variations, Cambridge: Cambridge Univ. Press, IAU Colloquium 143, p. 37

Neckel H., 1999, Sol. Phys. 184, 421

Neckel H., Labs D., 1984, Sol. Phys. 90, 205

Nesis A., Hanslmeier A., Hammer R., et al., 1992, A&A 253, 561

Nordlund Å., 1984, in S. Keil (ed.), Small-scale dynamical Processes in quiet stellar atmospheres, National Solar Observatory, Sunspot, New Mexico, p. 181

Nordlund Å., Dravins D., 1990, A&A 228, 155

Nordlund Å., Stein R., 1996, in Noels et al. (ed.), Proceedings of the 32nd Liège Int. Astrophys. Colloquium, Université de Liège, Institut d'Astrophysique, p. 75

Ploner S.R.O., Solanki S.K., Gadun A.S., 2000, A&A Submitted

Press W.H., Teukolsky S.A., Vetterling W.T., Flannery B.P., 1992, Numerical Recipies in Fortran, Cambride University Press, New York, 2nd ed.

Ruiz Cobo B., Del Toro Iniesta J.C., 1992, ApJ 398, 375

Ruiz Cobo B., Rodriguez Hidalgo I., Collados M., 1997, ApJ 488, 462

Schnabel R., Kock M., Holweger H., 1999, A&A 342, 610

Socas-Navarro H., Ruiz Cobo B., Trujillo Bueno J., 1998, ApJ 507, 470

Spruit H., Nordlund Å., Title A., 1990, ARA&A 28, 263

Stein R., Nordlund Å., 1998, ApJ 499, 914

Sugar J., Corliss C., 1985, J. Phys. Chem. Ref. Data 14, Suppl 2

Unsöld A., 1955, Physik der Sternatmosphären, Springer Verlag, Berlin, 2nd ed.

Vernazza J.E., Avrett E.H., Loeser R., 1981, ApJS 45, 635

Westendorp Plaza C., del Toro Iniesta J.C., Ruiz Cobo B., et al., 1997, Nat 389, 47

Westendorp Plaza C., del Toro Iniesta J.C., Ruiz Cobo B., et al., 1998, ApJ 494, 453